Cancer Immunology, Immunotherapy (2025) 74:50
https://doi.org/10.1007/s00262-024-03893-1

RESEARCH

Therapeutic effect of fully human anti-Nrp-1 antibody on non–small cell lung cancer in vivo and in vitro

Bo Zhang[1,4] · Qin Liu[1] · Lin Li[1] · Yingchun Ye[1] · Xiyuan Guo[1] · Wenfeng Xu[1] · Ligang Chen[3] · Xianming Mo[5] · Siji Nian[1] · Qing Yuan[1,2]

Received: 12 June 2024 / Accepted: 11 November 2024

Abstract

Although immune checkpoint inhibitors have changed the treatment paradigm for non-small cell lung cancer (NSCLC), not all patients benefit from them. Therefore, there is an urgent need to explore novel immune checkpoint inhibitors. Neuropilin-1 (Nrp-1) is a unique immune checkpoint capable of exerting antitumor effects through $CD8^+$ T cells. It is also a T-cell memory checkpoint that regulates long-term antitumor immunity. However, its role in NSCLC remains unclear. The aim of this study was to develop a fully human anti-Nrp-1 antibody with therapeutic effects against NSCLC in vitro and in vivo. We screened and constructed of a high-affinity anti-Nrp-1 IgG antibody from a constructed high-capacity fully human single-chain fragment variable (scFv) phage library. This novel anti-Nrp-1 IgG antibody partially restored the killing function of exhausted $CD8^+$ T cells in malignant pleural fluid in vitro. Co-culture of peripheral blood mononuclear cells (PBMC) with A549 and the addition of anti-Nrp1-IgG enhanced the killing of A549 target cells, leading to an increase in late-stage apoptosis of target cells. Importantly, anti-Nrp1-IgG treatment significantly reduced tumor volume in a mouse model of lung cancer with humanized immune system. These findings suggest that 53-IgG has a promising application as a potent Nrp-1-targeting agent in NSCLC immunotherapy.

Keywords NSCLC · Nrp-1 · IgG1 antibody · Tumor immunotherapy

✉ Siji Nian
sijinian@swmu.edu.cn

✉ Qing Yuan
qingyuan@swmu.edu.cn

1 Public Center of Experimental Technology, The School of Basic Medical Sciences, Southwest Medical University, Luzhou 646000, Sichuan Province, China

2 Institute of Nuclear Medicine, Southwest Medical University, Department of Nuclear Medicine, Affiliated Hospital of Southwest Medical University, Nuclear Medicine and Molecular Imaging Key Laboratory of Sichuan Province, Luzhou, China

3 Department of Neurosurgery, The Affiliated Hospital of Southwest Medical University, Sichuan Clinical Research Center for Neurosurgery, Luzhou 646000, Sichuan Province, China

4 Clinical Laboratory, Female and Child Health Care and Family Planning Service Center, Binhai New Area, Tianjin 300450, China

5 Department of Gastrointestinal Surgery, Laboratory of Stem Cell Biology, State Key Laboratory of Biotherapy, West China Hospital, Sichuan University, Chengdu 610041, China

Abbreviations

ECD	Extracellular segment gene fragment
HNSCC	Head and neck squamous cell carcinoma
ICIs	Immune checkpoint inhibitors
KD	Equilibrium dissociation constant
Nrp-1	Neuropilin-1
NSCLC	Non-small cell lung cancer
PBMCs	Peripheral blood mononuclear cells
PEMCs	Pleural effusion mononuclear cells
scFv	Single-chain fragment variable
SDS-PAGE	Sodium dodecyl sulfate-polyacrylamide gel electrophoresis
SOE PCR	Splicing by overlap extension PCR
TILs	Tumor-infiltrating lymphocytes; PCR: polymerase chain reaction
VEGF	Vascular endothelial growth factor
VEGFR2	Vascular endothelial growth factor receptor 2

Published online: 03 January 2025

Introduction

Lung cancer is the leading cause of cancer-related deaths globally. Despite employing surgical resection, radiotherapy, platinum-based chemotherapy, and targeted therapy, the overall effectiveness of these existing treatments remains severely limited [1, 2]. The discovery of immune checkpoints and the subsequent Nobel Prize-winning development of immune checkpoint inhibitors (ICIs) brought about a complete revolution in the treatment of lung cancer [3]. While nivolumab and pembrolizumab have emerged as extensively studied ICIs for lung cancer, the beneficiaries are still in the minority—only 20–30% of cancer patients respond to ICIs treatment [4, 5]. Consequently, there is a pressing need for the exploration of novel ICIs.

Nrp-1 emerges as a type I transmembrane protein [6]. Originally identified in neuronal and endothelial cells, its crucial roles encompass normal embryonic development, axon guidance, and vascular system formation [7–9]. Nrp-1 is also expressed by various immune cells and actively participates in immune function [10]. Within the realm of cancer immunotherapy, Nrp-1 represents a promising immune checkpoint. In the tumor microenvironment, Nrp-1 exerts co-suppressive effects on antitumor immunity by modulating CD8 T cells and Treg cells, often coexisting with multiple other immune checkpoints [11, 12]. Furthermore, Nrp-1 functions as a T-cell memory checkpoint, restricting long-term antitumor immunity and influencing T-cell memory development specific to tumor antigens [13]. This pivotal role of Nrp-1 in tumor immunity renders it an enticing immune checkpoint, thereby underscoring the research potential of monoclonal antibodies targeting Nrp-1.

Currently, there are no U.S. Food and Drug Administration–approved anti-Nrp-1 antibody drugs, and clinical studies of Nrp-1 antibody have focused on its role in tumor angiogenesis through interaction with VEGFR2 co-receptors. A phase I study of a human monoclonal anti-Nrp-1 antibody (MNRP1685A) in patients with advanced solid tumors confirmed its tolerability as a stand-alone agent, albeit with limited clinical efficacy [14]. A dual-targeted, bispecific antibody against VEGFA and Nrp-1 (IDB0076) was preliminarily evaluated for pharmacotoxicity in crab-eating monkeys and showed no significant adverse effects, but has not yet been subjected to clinical studies for further development [15]. Only one anti-Nrp-1 monoclonal antibody is currently undergoing clinical evaluation to assess its inhibitory effect on Treg cell function in combination with nivolumab in patients with advanced solid tumors (NCT03565445), and the results have not been reported.

This study elucidated the upregulation of Nrp-1 gene expression on tumor-infiltrating lymphocytes (TILs) $CD8^+$ T cells within tumor tissues of patients with lung adenocarcinoma. Employing a large-capacity full-human scFv phage library, we successfully screened high-affinity scFv molecules targeting Nrp-1. Subsequently, we constructed a full-length IgG antibody and achieved stable expression and purification. In vivo and in vitro experiments unequivocally demonstrate the anti-Nrp-1 IgG antibody's capacity for tumor suppression, laying a solid foundation for future tumor immunotherapy endeavors.

Materials and methods

Cell lines and cell culture

HEK293F cells and CHO-S cells were procured from Thermo Fisher Scientific (USA), while Jurkat T cells and A549 cells were obtained from ATCC (USA). HEK293F cells were maintained as suspension cells in the HEK 293F complete medium (Sino Biological Inc., China), while CHO-S cells were cultured in suspension using ExpiCHO™ Expression Medium (Gibco, USA). Jurkat T cells and A549 cells were cultured in RPMI-1640 medium (Gibco, USA) supplemented with 10% FBS (HyClone, USA) and 1% penicillin and streptomycin (Solarbio, Beijing, China). All cell cultures were maintained at 37 °C in a 5% CO_2 cell culture incubator.

Specimen handling and flow cytometry

PBMCs and pleural effusion mononuclear cells (PEMCs) were isolated from patients with lung adenocarcinoma (the patient information is summarized in supplementary Information Table 1) using a human peripheral blood lymphocyte isolation solution (Cytiva, USA). Fresh lung adenocarcinoma tumor tissues were dissociated into single cells using a combination of enzymes and a fully automated tissue single-cell processor (Miltenyi, USA).

For human cell surface staining, we used FITC anti-Human CD3 antibody, APC/Cyanine7 anti-Human CD8 antibody, PE/Cyanine7 anti-human CD304 (Neuropilin-1) antibody, APC anti-human PD1 antibody, and PE anti-human TIM3 antibody (all from Biolegend, USA). We employed 7AAD (BD, USA) to exclude dead cells, and flow cytometry (ACEA, USA) was utilized for analysis.

Nrp-1 antigen protein construction and expression

The Nrp-1 gene sequence (GenBank accession number: NM_001024629.2) was retrieved from the NCBI database. We selected the amino acid sequence spanning positions 22–644 of the extracellular segment (SEQ ID No. 16). The gene fragment of the extracellular segment of Nrp-1 was

amplified through PCR under the following conditions: 98 °C for 10 s, 60 °C for 30 s, and 68 °C for 2 min, with a total of 30 cycles. Subsequently, it was ligated into the pcDNA3.4 vector, and the endotoxin-free plasmid was extracted. The antigen was expressed in HEK293F cells following transient transfection using polyethyleneimine (PEI), and the supernatant was collected after seven days. Purification was carried out using a nickel affinity chromatography column (GE, USA), and the purification was verified through SDS-PAGE.

Construction of phage antibody immunolibrary

Extraction of total RNA from lymphoid tissues of non–small cell lung cancer patients and PCR amplification of light and heavy chains

Total lymphocyte RNA from NSCLC (the patient information is summarized in supplementary Information Table 1) lymphoid tissues was extracted using TRIzol reagent (TaKaRa, Japan), and first-strand cDNA was synthesized through reverse transcription using oligodeoxynucleotides (dT) as primers. Primer sequence combinations were designed based on the heavy and light chain framework regions of human antibody sequences (for primer sequences, see [15]). The coding regions of the heavy chain variable structural domains (VH) and light chain variable structural domains (VL, including Vλ and Vκ) of the antibody fragments were amplified using the PCR. PCR reaction conditions were as follows: 94 °C for 30 s, 55 °C for 30 s, and 72 °C for 30 s, for a total of 30 cycles. Purified VH or VL DNA from different patients was combined for subsequent VH and VL splicing.

Construction of a fully human scFv phage library

Purified VH and VL were utilized as templates for splicing into scFv through overlapping PCR amplification. The scFv fragment included Sfi I and Not I restriction sites. The first round of overlapping extension PCR was conducted under the following conditions: no primer, 94 °C for 1 min, 68 °C for 1 min, for 20 cycles. The product from the first round of PCR was used as the template for the second round of PCR, using the upstream primer VHFvF and the downstream primer VλFvR or VκFvR. The second round of PCR was performed at 94 °C for 1 min, 55 °C for 1 min, and 72 °C for 1 min, for 30 cycles.

The scFv library genes were generated by combining VH-linker-Vκ and VH-linker-Vλ. These scFv library genes, along with the pCANTAB5E vector plasmid, were digested with the Sfi I and Not I restriction endonucleases, respectively. Subsequently, they were ligated and transformed into TG1 receptor cells, followed by overnight incubation at 37 °C on LBAG solid medium to assess library capacity. To evaluate the diversity of the scFv library, we randomly selected 20 single colonies from the library for PCR identification. The PCR products were then digested with BstN I to create DNA fingerprints.

Anti-Nrp-1-scFv three rounds of enrichment and affinity screening

Next, the amplified library phages were incubated with containment buffer (containing 3% fetal bovine serum albumin [BSA]) for 1 h at room temperature. We added 2 μg of biotinylated Nrp-1 protein to the closed library phage and incubated it for 2 h at room temperature. The phage antigen–antibody complexes were captured using streptavidin-labeled Dynabeads M-280 and washed with 5 × phosphate-buffered saline with Tween 20 (PBST). Phages were eluted with 0.1 M glycine–HCl (pH = 2.2), followed by neutralization to pH 7.0 with 1 M Tris. These eluted phages were subsequently infected into logarithmically growing TG1 cells and spread on LBAG plates, after which the colonies were harvested the next day for the next round of screening, for a total of three rounds.

After three rounds of screening, single colonies were randomly selected from the enriched scFv phage library, and phages were amplified to express scFv in small quantities. We used an ELISA to detect the expressed phage scFv. The purified Nrp-1 protein was diluted to 2 μg/mL with coating buffer (0.1 M $NaHCO_3/Na_2CO_3$) and then coated on the plastic surface of a 96-well microtiter plate at 4 °C overnight. After washing three times with washing buffer (1 × phosphate-buffered saline [PBS] containing 0.05% Tween-20) for 5 min each time, ELISA blocking solution (containing 5% skim milk powder) was added to the wells, and the plate was incubated at 37 °C for 1 h. After washing, phage supernatant containing the containment solution was added to the wells, and the plate was incubated for 1 h at 37 °C. After additional washing, an anti-M13/horseradish peroxidase (HRP) antibody (1/5000; Abcam, UK) was added, and the mixture was left at room temperature for 1 h. The color development reaction was initiated by adding tetramethylbenzidine substrate (Thermo Fisher Scientific, USA) to each well, and the reaction was halted with 2 N H_2SO_4. The results were read at OD_{450} using a microplate reader (Thermo Fisher Scientific, USA).

Construction and expression of anti-Nrp-1 IgG

The screened anti-Nrp-1-scFv with good binding activity and specificity was used as a template to amplify VH and VL by PCR. The primer sequences in Table 2 were used in this study. VH and VL were then inserted through PCR homologous recombination into the pcDNA3.4/SP-CH and

pcDNA3.4/SP-CL vectors, both of which were constructed in our laboratory (pcDNA3.4/SP-CH is a plasmid that contains the human IgG1 heavy chain constant region gene, and pcDNA3.4/SP-CL contains the human κ light chain constant region gene.). These constructs were subsequently transformed into *E. coli* TOP 10 receptor cells. The plasmids were extracted using an endotoxin-free pellet kit after correct sequencing (Tiangen, China), and anti-Nrp-1-IgG1 protein was expressed in CHO-S eukaryotic cells following transfection using a transfection kit (Thermo Fisher Scientific, USA). On day 14 of expression, the supernatant was collected and centrifuged at 8,000 rpm for 10 min, after which the antibody was purified from the supernatant using a protein A affinity chromatography column (GE, USA).

Detection of antigen–antibody affinity

To determine the binding affinity of anti-Nrp-1 IgG antibody to Nrp-1 protein, we employed the BioLayer Interference (BLI) technique. Biotinylated Nrp-1 protein (10 μg/mL) was coupled to a SA biosensor (Pall ForteBio, USA). Subsequently, 200 μL of purified anti-Nrp-1 IgG antibody (0, 5, 10, and 20 μg/mL) was added to the biosensor to assess antigen–antibody interactions. KD values were calculated by systematically analyzing antigen–antibody binding and dissociation.

Detection of anti-Nrp1 IgG1 binding to cells by flow cytometry

Establishment of A549 and Jurkat cells overexpressing the Nrp-1 gene

Lentiviruses containing the Nrp-1 gene (MOI = 40, Obio Technology, China) were used to infect A549 and Jurkat T cells in logarithmic growth phase. Polybrene was added at a final concentration of 5 μg/mL, and the cells were cultured at 37 °C in a 5% CO_2 cell culture incubator. After 12–16 h of infection, the medium was replaced. Following 72–96 h of infection, the cells were observed using fluorescence microscopy (Olympus, Japan), and the infection rate was verified through flow-through analysis.

Nrp-1 lentivirus-infected A549 and Jurkat T cells were used, and empty carrier cells were utilized as the control group. The cells were lysed using cell lysis solution (Beyotime, China) and separated via 12% SDS-PAGE. The separated products were then transferred to PVDF membranes and sealed with a sealing solution (PBST containing 5% skim milk powder) at room temperature for 1 h. Subsequently, anti-Nrp-1 antibody (1/1500; Abcam, UK) and anti-GAPDH antibody (1/800; Abcam, UK) were added and incubated at room temperature for 1 h. The membranes were washed five times with PBST for 5 min each. HRP-labeled sheep anti-rabbit antibody (1/8000; Bioss, China) and sheep anti-mouse antibody (1/1000; Beyotime, China) were added, and the membranes were incubated at room temperature for 1 h. After another five washes with PBST, color development was initiated using ECL (Beyotime, China).

Detection of anti-Nrp-1-IgG1 and cell binding activity by flow cytometry

Stable cell lines (Jurkat T and A549) expressing Nrp-1 on the cell membrane surface were cultured. When the cells reached the logarithmic growth phase, they were either digested with 0.25% trypsin or directly centrifuged and washed with a PBS solution. The cell count was adjusted to 1×10^5 cells per tube. Anti-Nrp1 IgG1 was diluted to 40 μg/mL, and 100 μl of anti-Nrp-1 IgG at different concentrations was prepared through pairwise dilution and added to the corresponding cells. The cells were then incubated at 4 °C for 30 min. Alexa Fluor 647 antibody (1/500; Bioss, China) was added, and the mixture was incubated at 4 °C for another 30 min. After two washes, the cell suspension was collected in 1 × PBS for flow cytometry analysis.

Effect of anti-Nrp1 IgG1 on memory T cells and antitumor activity detected from cellular level

Effect of anti-Nrp1 IgG on depleted $CD8^+$ T cells in malignant pleural effusion detected by flow cytometry

PEMCs isolated from the malignant pleural fluid of patients with lung adenocarcinoma were stimulated with a final concentration of 1 μg/mL anti-CD3/CD28 antibody (Ultra-LEAFTM Purified anti-human CD3, Ultra-LEAFTM Purified anti-human CD28, Biolegend, USA) for 3 days [16] [17] [18]. These cells were then seeded in 48-well plates, either with or without the addition of a final concentration of 40 μg/mL 31-IgG, 53-IgG, or anti-PD-1 antibody (Nivolumab, Selleck, USA). Each well contained 1 mL of the cell suspension, and incubation took place at 37 °C in a 5% CO_2 cell incubator for 3 days. The cells were collected for flow cytometry analysis of apoptosis. In the same way, cells were collected for immune memory analysis of $CD8^+$ T cells. BV510 anti-human CD45RA Antibody and BV421 anti-human CCR7 Antibody were from Biolegend, USA.

CCK8 assay

A549 cells were evenly seeded into 96-well plates at a density of 6×10^4 cells/mL at 100 μL per well. The experimental wells, blank control wells, and negative control wells were established according to the CCK8 reagent instructions. The 96-well plate was incubated in an incubator at 37 °C with 5% CO2 for 24 h. After the medium was discarded, the final concentration of 53 IgG1 antibody at 25 μg/mL, 50 μg/mL,

and 100 µg/mL was added to the experimental wells at 100 µL per well. Next, 10 µL of CCK8 reagent (APE × BIO, Houston, USA) was added to each well at 24 h, 48 h, and 72 h post-incubation. The absorbance at 450 nm was measured using an enzyme marker after a 1 h incubation.

Flow cytometry detection of anti-Nrp-1 IgG1 killing of target cells using PBMCs

A549 cells were used as target cells. When the cells were in the logarithmic growth phase, they were detached from the culture dish and resuspended in RPMI 1640 medium containing 10% FBS. The cells were labeled by adding a final concentration of 2.5 µM CFSE (BioLegend, USA) and seeded in a 96-well cell culture plate at a density of 2×10^4 cells per well. The plate was placed in a cell incubator for 24 h. Meanwhile, PBMCs isolated from healthy donors were used as effector cells and stimulated with anti-CD3/CD28 antibody for three days. Effector and target cells were added to the 96-well cell culture plates at a ratio of 10:1, with the final concentration of effector cells being 2×10^5 cells per well, with or without the addition of a final concentration of 40 µg/mL of 31-IgG, 53-IgG, or anti-PD-1 antibody (nivolumab) [17] [19] [20] [21]. Each well contained 200 µL of the solution. The 96-well plates were placed in a 37 °C, 5% CO_2 cell incubator for 48 h. Cells were collected for flow cytometry analysis of apoptosis in the target cells.

Detection of antitumor activity of anti-Nrp1 IgG1 in vivo

Female NTG mice (derived from the CB-17/Icr mouse (BALB/c homolog), severe combined immunodeficient mice lacking mature T cells, B cells and NK cells, at 6 weeks of age were maintained in an SPF environment for 1 week to acclimate. A549 cells were injected into the right rib cage of the mice at a density of 2×10^6 cells per injection. The tumor volume was measured every 2–3 days and calculated using the formula: tumor volume (mm^3) = $1/2 \times \text{length} \times \text{width}^2$. When the tumor volume reached approximately 80 mm^3, human PBMCs were injected into the tail vein at a density of 2×10^7 cells per mouse [22] [23] [24]. Subsequently, 53-IgG1 was injected intraperitoneally on the following day of the PBMC injection. Human IgG1 was used in the control group, with an antibody dosage of 10 mg/kg and 100 µL per mouse. The mice received intraperitoneal injections of the antibody every 2 days for a total of five injections. The mice were euthanized after blood was collected from their eye sockets on the day following the last administration. Tumors were dissected, weighed, and photographed to extract TILs, which were analyzed by flow assay using PE anti-human CD45 Antibody (BD, USA), FITC anti-Human CD3 Antibody (Biolegend, USA), and APC/Cyanine7 anti-human $CD8^+$ antibody (Biolegend, USA) fluorescent antibodies. 7AAD (BD, USA) was used to exclude dead cells, and TILs in tumor tissues were analyzed using flow cytometry.

Statistical analysis

Statistical analysis was conducted using Prism 8 (GraphPad software). The data are expressed as the mean ± standard deviation, and t-tests were employed for between-group comparisons of normally distributed data. The Mann–Whitney U test was used for non-normally distributed data. A significance level of $P > 0.05$ was considered not statistically significant (ns), while $^*P < 0.05$, $^{**}P < 0.01$, and $^{***}P < 0.001$ were considered to indicate statistical significance.

Results

Construction of a fully human scFv phage immunization library

Total RNA was extracted from lymphoid tissues of 20 patients with NSCLC to perform reverse transcription to cDNA. The amplified gene bands of VH, Vλ, and Vκ libraries were approximately 400 base pairs in size (Fig. 1a–c). The purified amplification products of VH, Vλ, and Vκ from different patients were then mixed in equal proportions. To create the VH-linker gene library, a Sfi I site was added to the upstream primer, and the splice sequence was added to the downstream primer. Similarly, the Vλ-linker and Vκ-linker gene libraries were constructed by adding the splice sequence to the upstream primer and the Not I site to the downstream primer, respectively. The VH-linker-VL gene library, approximately 800 base pairs in size (Fig. 1d), was obtained through gene splicing by overlap extension PCR (SOE PCR), resulting in the successful construction of a fully human scFv phage immunization library.

Subsequently, DNA from the scFv library was ligated with the phage vector pCANTAB5E and transformed into Escherichia coli TG1. We randomly selected 20 monoclonal colonies for the identification of the scFv insert fragments using polymerase chain reaction (PCR). The results demonstrated that all monoclonal colonies contained the full-length scFv gene (Fig. 1e). DNA fingerprinting by BstN I enzyme cleavage of scFv DNA revealed distinct patterns for each scFv (Fig. 1f). These constructed human scFv phage immune libraries are diverse, and the gene sequences within the antibody libraries are enriched.

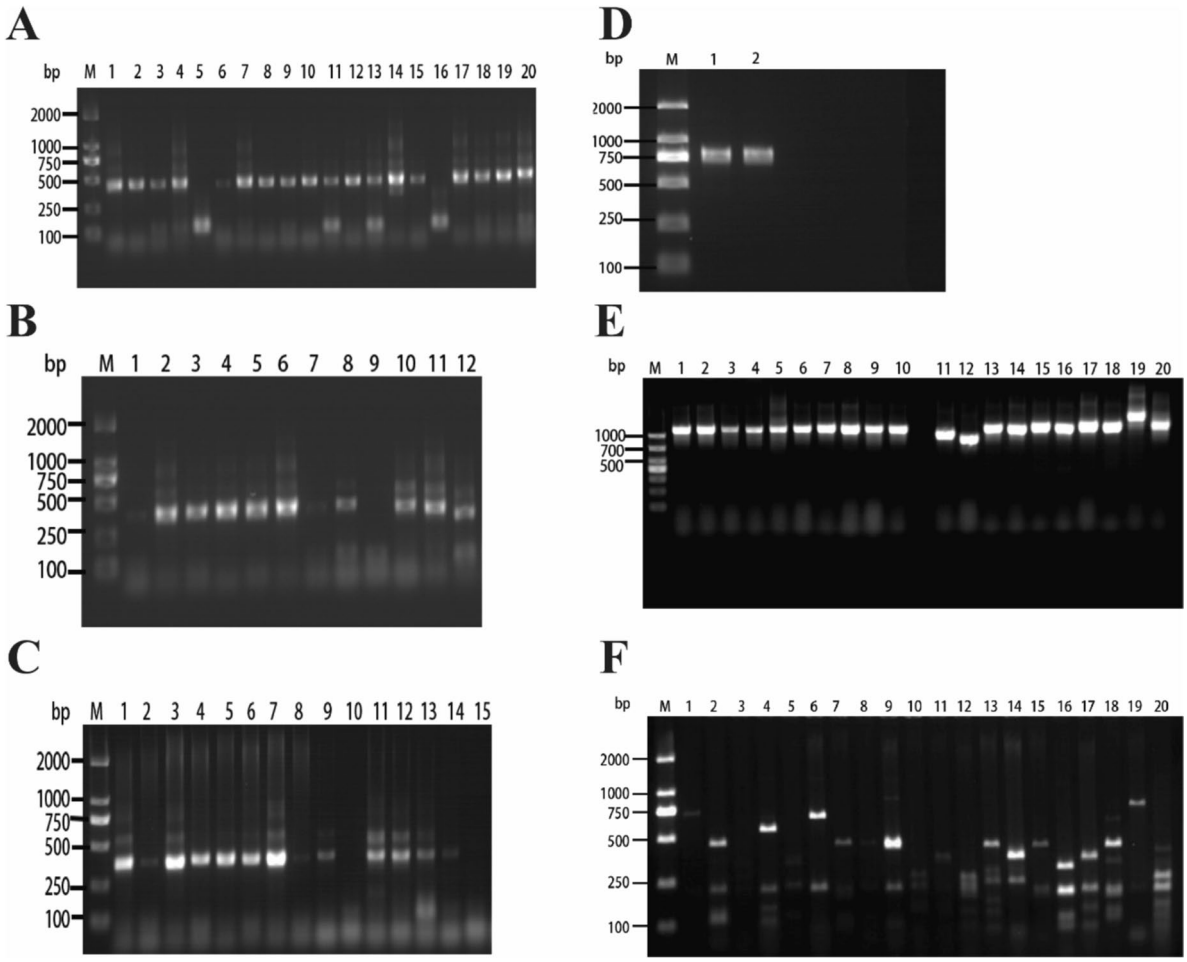

Fig. 1 Construction and diversity analysis of scFv phage antibody immunolibrary. **a** M represents a DNA marker of DL2000 base pairs, and bands 1–20 indicate amplified VH gene bands. **b** M represents a DNA marker of DL2000 base pairs, and bars 1–12 represent amplified Vκ gene bands. **c** M represents a DNA marker of DL2000 base pairs, and 1–15 indicate amplified Vλ gene bands. **d** M represents a DNA marker of DL2000 base pairs, where 1 is the amplified VH-Vκ gene band, and 2 is the amplified VH-Vλ gene band. **e** Insertion rate of the full-length scFv gene in the phage library, M represents the DL1000 base pairs DNA marker, and 1–20 indicate different monoclonals randomly selected from the phage library. **f** DNA fingerprinting of scFv in the phage library. M represents the DL2000 base pairs DNA marker, and 1–20 represent different monoclonal colonies in the phage library

Nrp-1 expression in lung adenocarcinoma and healthy donor CD8$^+$ T cells

Upon analyzing the expression of Nrp-1 on PBMCs and TIL CD8$^+$ T cells from patients with lung adenocarcinoma, we discovered that Nrp-1 was expressed at a significantly higher frequency on TIL CD8$^+$ T cells compared to PBMCs ($P < 0.01$; Fig. 2a). Meanwhile, we compared the correlation of Nrp-1 expression with PD1 and TIM3 in peripheral blood PBMCs and CD8$^+$ T cells in tissues from tumor patients, respectively. The results showed that Nrp-1$^+$CD8$^+$ T cell frequency was positively correlated with PD1$^+$CD8$^+$ T cells and TIM3$^+$CD8$^+$ T cells (Fig. S1a and b). Furthermore, we evaluated the expression of Nrp-1 on CD8$^+$ T cells in an activated state of PBMCs from healthy donors. The results indicated that anti-CD3/CD28 monoclonal antibody-stimulated PBMCs displayed an increased cell frequency compared to the unstimulated group ($P < 0.01$; Fig. 2b). These findings suggest that Nrp-1 expression is elevated on activated and exhausted CD8$^+$ T cells but low on unactivated CD8$^+$ T cells, suggesting that the Nrp-1 gene is a promising target for exploration.

Construction of Nrp-1 extracellular segment protein expression vector and purification of Nrp-1 expression

The Nrp-1 gene sequence (NM_001024629.2) was retrieved from the NCBI database. The amino acid sequence spanning positions 22–644 of the extracellular segment was selected, with a His tag added at the C-terminus. The Nrp-1 extracellular segment gene fragment (ECD) was obtained through

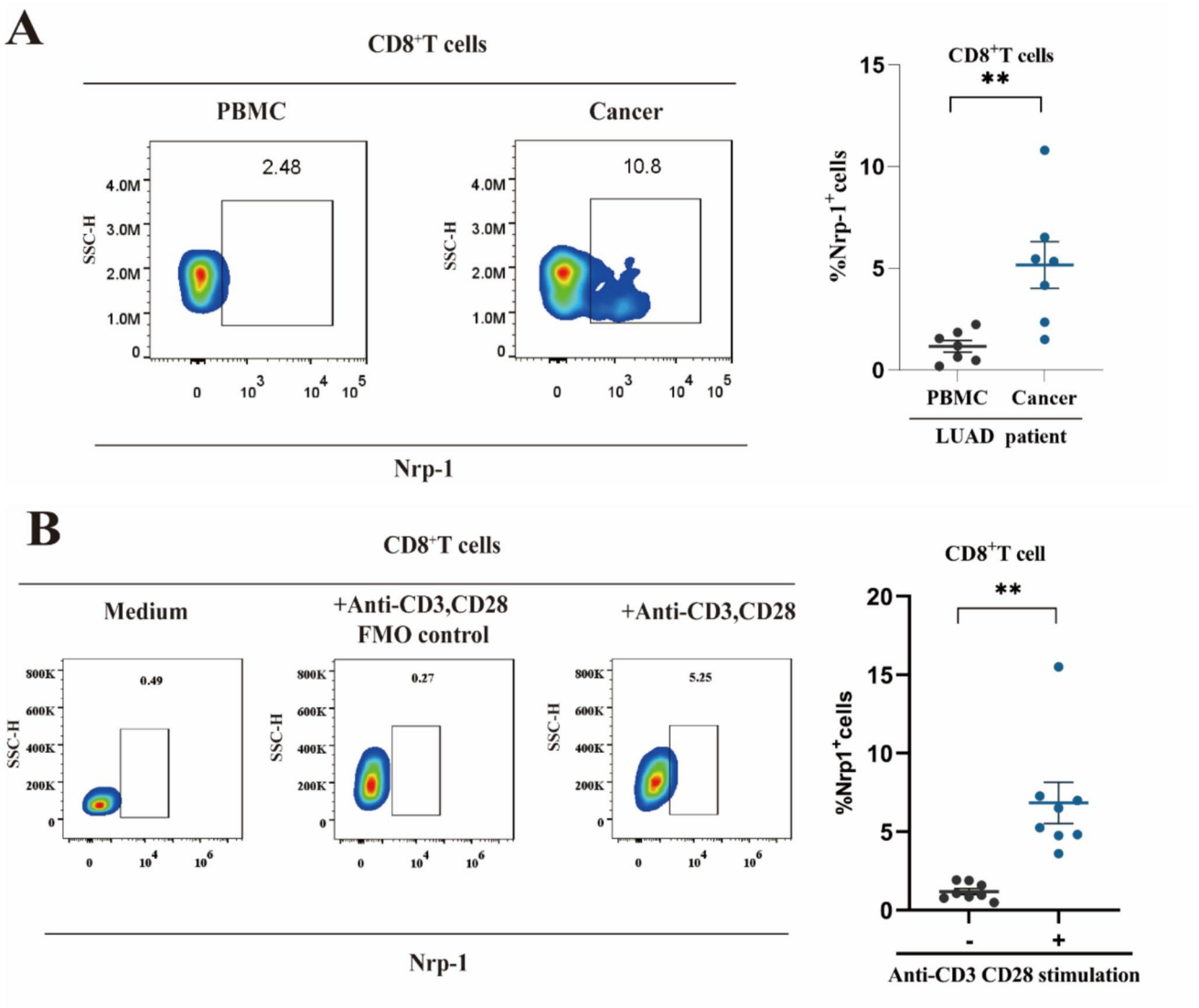

Fig. 2 Expression of Nrp-1 in lung adenocarcinoma and healthy donor CD8$^+$ T cells. **a** Left: Cell flow scatter plot analysis of Nrp-1 expression on the upper surface of CD8$^+$ T cells from PBMCs and TILs in patients with lung adenocarcinoma. Right: Percentage of Nrp-1 in CD8$^+$ T cells. Patients with lung adenocarcinoma, n = 7 **b** Left: Cell flow scatter plot analysis of Nrp-1 expression on the surface of CD8$^+$ T cells in the PBMC unstimulated, anti-CD3/CD28 antibody-stimulated FMO control and anti-CD3/CD28 antibody-stimulated groups of healthy donors. Right: Percentage of Nrp-1 in CD8$^+$ T cells, where healthy donors $n = 8$. * $P < 0.05$, ** $P < 0.01$, *** $P < 0.001$

PCR amplification, with agarose gel electrophoresis confirming a fragment size of approximately 1900 base pairs (Fig. 3a). Subsequently, the Nrp-1 gene fragment was ligated with the pcDNA3.4 vector and transformed into *E. coli* TG1. Colony PCR amplification of randomly selected single clone colonies indicated a gene fragment size of about 2000 base pairs (Fig. 3b), and gene sequencing confirmed the successful construction of the Nrp-1 extracellular segment protein expression vector.

The constructed expression vector was transiently transfected into HEK293F eukaryotic cells, and the supernatant containing the recombinant protein was collected on day 7 of expression. The protein was purified using nickel column affinity chromatography. Sodium dodecyl sulfate–polyacrylamide gel electrophoresis (SDS-PAGE) results confirmed the successful purification of the target protein, with the Nrp-1 extracellular segment protein measuring approximately 75 kDa in size (Fig. 3c).

Screening of anti-Nrp-1 scFvs and construction of anti-Nrp-1 IgG1 and its expression

The biotinylated Nrp-1 ECD protein was introduced to an amplified scFv immune library using a liquid-phase

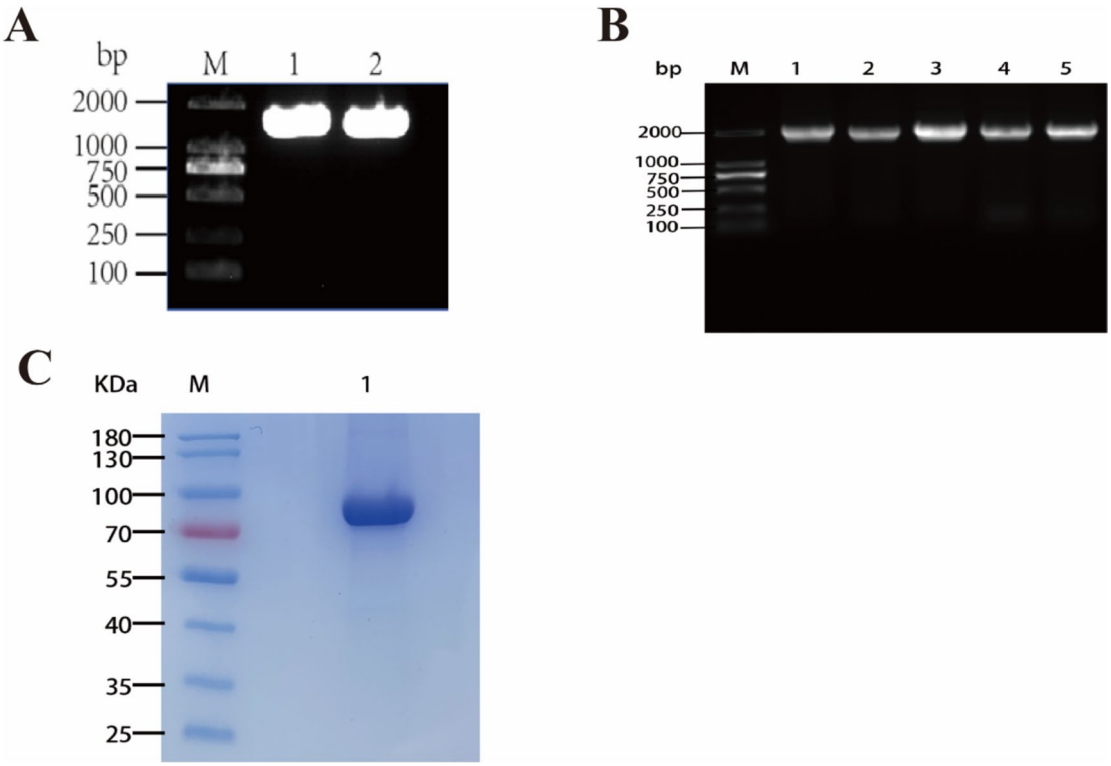

Fig. 3 Construction of Nrp-1 extracellular segment protein expression vector and purification of Nrp-1 expression. **a** M is the DNA marker of DL2000 base pairs, and 1 and 2 represent the amplified Nrp-1 extracellular segment gene bands. **b** M is the DNA marker of DL2000 base pairs, PCR verification of Nrp-1 gene fragment inserted into pcDNA3.4 vector, and 1–5 represent the positive amplification of colony PCR **c** M is the protein marker, and 1 represents the purified band of Nrp-1 extracellular segment protein

screening approach. The resulting phage antigen–antibody complexes were captured using streptavidin-coated Dynabeads M-280. Following three rounds of enrichment through phage display technology, monoclonal colonies were randomly selected from the libraries screened during the third round. The scFv DNA was subsequently digested using the BstN I enzyme, and DNA fingerprinting demonstrated a decrease in diversity and an increase in specificity of scFvs targeting the anti-Nrp-1 ECD antigen after three rounds of enrichment and affinity screening (Fig. 4a–b).

After the completion of three rounds of enrichment screening, 248 monoclonal colonies were randomly chosen for small-scale expression of scFv. The binding activity of the secondary phage antibody library to the target antigen Nrp-1 ECD, following three rounds of enrichment affinity screening, was assessed using enzyme-linked immunosorbent assay (ELISA). A total of 30 monoclones displayed optical density (OD) values exceeding 1.4 (Fig. 4c). These monoclones exhibited high-affinity binding to the target antigen Nrp-1 ECD, with OD values for positive reactions surpassing two times the negative values.

The anti-Nrp-1 scFvs, characterized by correctly sequenced genes and distinct sequences, were designed with specific primers. Subsequently, the VH and VL fragments of the anti-Nrp-1 scFvs were amplified using PCR, with the VH fragment measuring approximately 350 base pairs and the VL fragment about 325 base pairs (Fig. 4d). These fragments were then inserted into a pcDNA3.4 vector containing human IgG CH, Cλ, and Cκ regions, as previously constructed in the laboratory, through homologous recombination. The resulting recombinant products were transformed into E. coli and cultured overnight, followed by the selection of single clones for PCR identification. The amplification results were confirmed through agarose gel electrophoresis. It was determined that the amplified VH, Vλ, and Vκ fragments, including some vector sequences, measured approximately 700 base pairs (Fig. 4e). This confirmed the successful amplification of VH and VL fragments of the anti-Nrp-1 scFv and the generation of the anti-Nrp-1-IgG1 antibody.

The constructed H-chain and L-chain expression vectors were transiently cotransfected into CHO-S eukaryotic cells, and the supernatant containing recombinant protein was collected on day 14 of expression. The supernatant was subsequently purified and recovered using protein A agarose gel. SDS-PAGE analysis confirmed the successful purification of the target protein. The sizes of

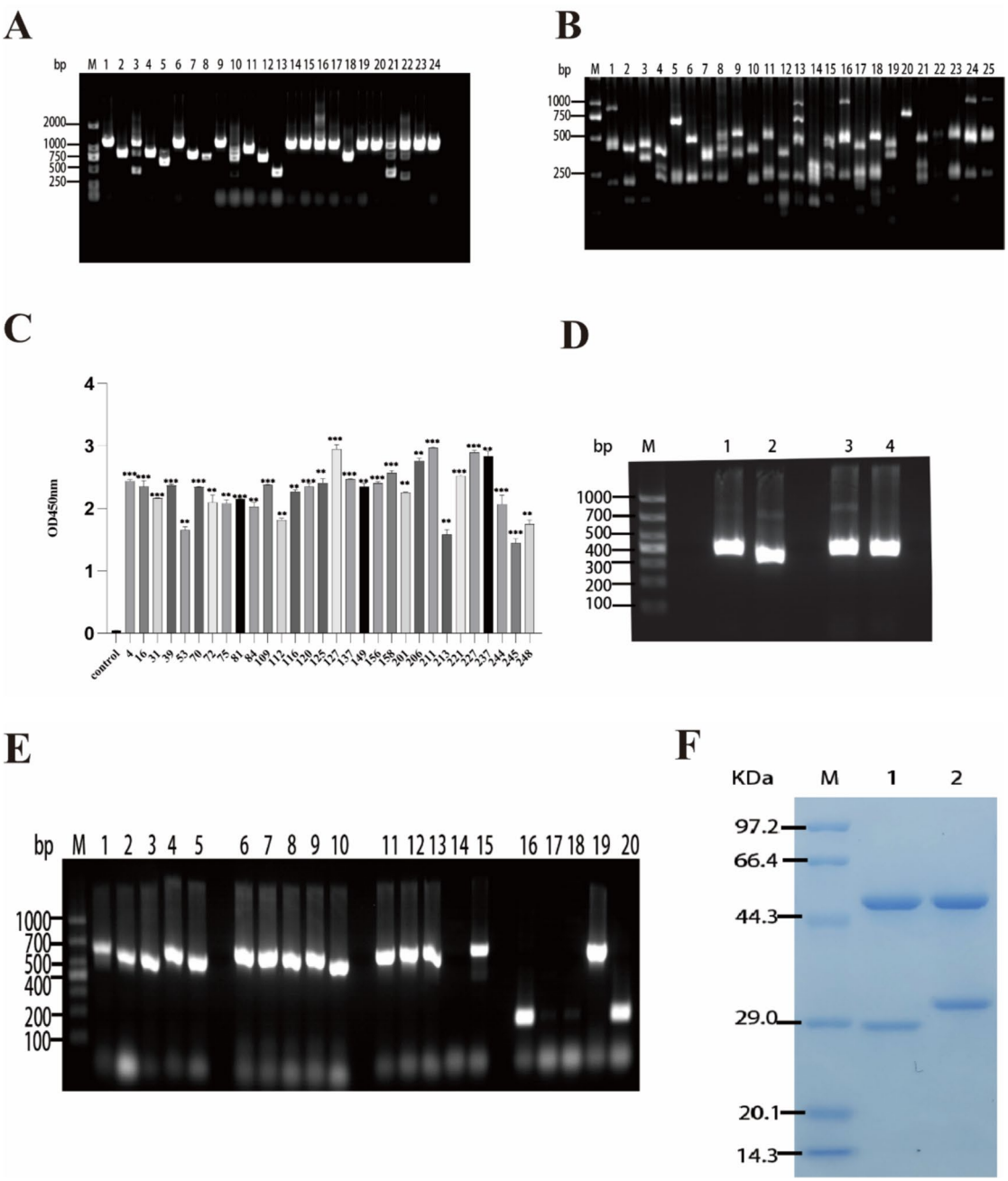

Fig. 4 Screening of high-affinity scFvs and expression of anti-Nrp-1 IgG1. **a** Insertion rate of phage library anti-Nrp-1 scFv gene, M is the DNA marker of DL2000 base pair, and 1–24 represent the numbers of different monoclonal colonies in the phage library. **b** Fingerprints of the phage library for the anti-Nrp-1 scFv gene, M is the DNA marker of DL1000 base pair, and 1–25 represent the numbers of different monoclonal colonies in the phage library. **c** Positive scFvs from a three rounds screened anti-Nrp-1 scFv phage library were subjected to ELISA to detect binding to antigen. **d** Amplification of VH and VL fragments of anti-Nrp-1 scFvs, M is the DNA marker of DL1000 base pair, 1–2 represent the amplified fragments of VH and Vλ for 31 scFv, respectively. 3–4 represent amplified fragments of VH and Vκ for 53 scFv, respectively. **e** VH and VL were inserted into SP-CH/pcDNA3.4, SP-CL/pcDNA3.4 vectors, and M was a DL1000 base pair DNA marker. 1–5 are 31-CH (containing part of the vector sequence), 6–10 are 31- Cλ (containing part of the vector sequence), 11–15 are 53 CH (containing part of the vector sequence), and 16–20 are 53-Cκ (containing part of the vector sequence) for PCR-validated insertion of the vector. **f** SDS-PAGE results of anti-Nrp-1-IgG1 recombinant protein. M is the protein marker, 1–2 are 31-IgG1, and 53 -IgG1 bands after purification, respectively

the anti-Nrp-1-IgG1 full antibody heavy chain and light chain were approximately 55 kDa and 25 kDa, respectively (Fig. 4f).

Anti-Nrp-1-IgG1 antigen binding affinity assay

The binding and dissociation of the antigen–antibody interactions were analyzed using biofilm interferometry. Affinity dissociation constants (KD = Kd/Ka) were calculated, revealing that both strains of fully human single-chain antibodies (31-IgG1 and 53-IgG1) exhibited high-affinity binding to the Nrp-1 target antigen. The results (Fig. 5a–b) indicated that the equilibrium dissociation constant (KD) value for 31-IgG1 was 9.207e-9, while that for 53-IgG1 was 2.68e-8. Consequently, 31-IgG1 and 53-IgG1 displayed a strong binding affinity to the Nrp-1 target antigen at the protein level, with 31-IgG1 exhibiting a higher binding affinity to the antigen.

Jurkat T and A549 cell lines were infected by Nrp-1 lentivirus for 48 h FCM results showed that Nrp-1 lentivirus successfully infected Jurkat T and A549 cell lines (Fig. S2a-S2b). At the same time, Western-blot results showed that Nrp-1 protein was expressed in Jurkat T cell line and A549 cell line (Fig. S3a-S3b). We conducted a detailed examination of the binding activity of anti-Nrp-1-IgG1 to Jurkat T and A549 cell lines, which were overexpressing Nrp-1, at the cellular level using flow cytometry. The binding results with Jurkat T cells overexpressing Nrp-1 are shown in Fig. 5c–d: 31-IgG1 exhibited a maximum binding rate of 40.2% to Jurkat T cells overexpressing Nrp-1, while 53-IgG1 showed a higher maximum binding rate

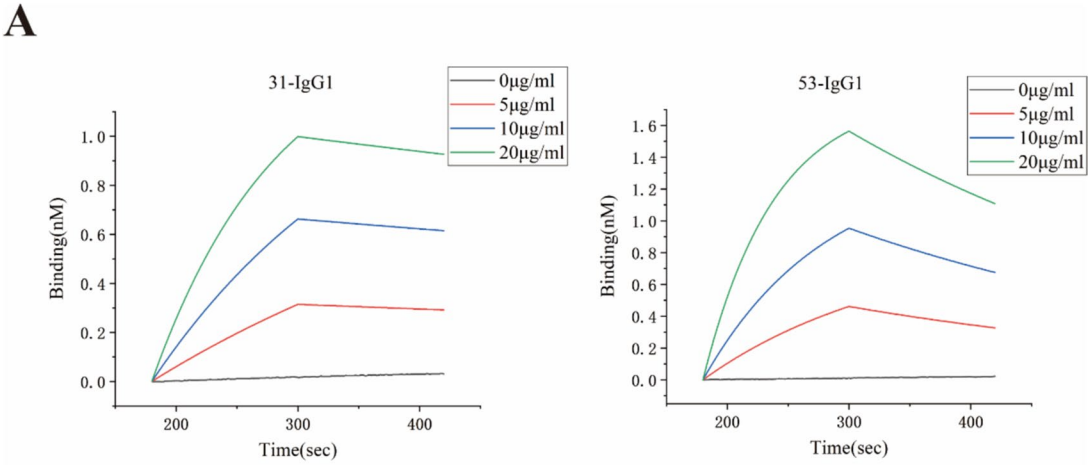

B

Antibody number	KD(M)	Ka(1/Ms)	Kd(1/s)
31	9.207e-9	6.792e4	6.253e-4
53	2.69e-8	1.069e5	2.875e-3

Fig. 5 Anti-Nrp1-IgG1 affinity assay for antigen binding. **a** Binding and dissociation curves of 31-IgG1 and 53-IgG1 with biotin-labeled Nrp-1 protein detected by biofilm interferometry. **b** Affinity analysis of 31-IgG1 and 53-IgG1 binding to biotin-labeled Nrp-1 proteins. "kd" stands for equilibrium dissociation constant; "Ka" stands for binding constant; "Kd" stands for dissociation constant. **c** The left panel displays the binding of different concentrations of 31-IgG1 to Nrp-1 on Nrp-1 overexpressing Jurkat T cells. The right panel shows the change in its average fluorescence intensity. **d** The left panel displays the binding of different concentrations of 53-IgG1 to Nrp-1 on Nrp-1 overexpressing Jurkat T cells. The right panel shows the change in its mean fluorescence intensity. **e** The left panel displays the binding of different concentrations of 31-IgG1 to Nrp-1 on Nrp-1 overexpressing A549 cells. The right panel shows the change in its average fluorescence intensity. **f** The left panel displays the binding of different concentrations of 53-IgG1 to Nrp-1 on Nrp-1 overexpressing A549 cells. The right panel shows the change in its average fluorescence intensity. The data came from three independent experiments

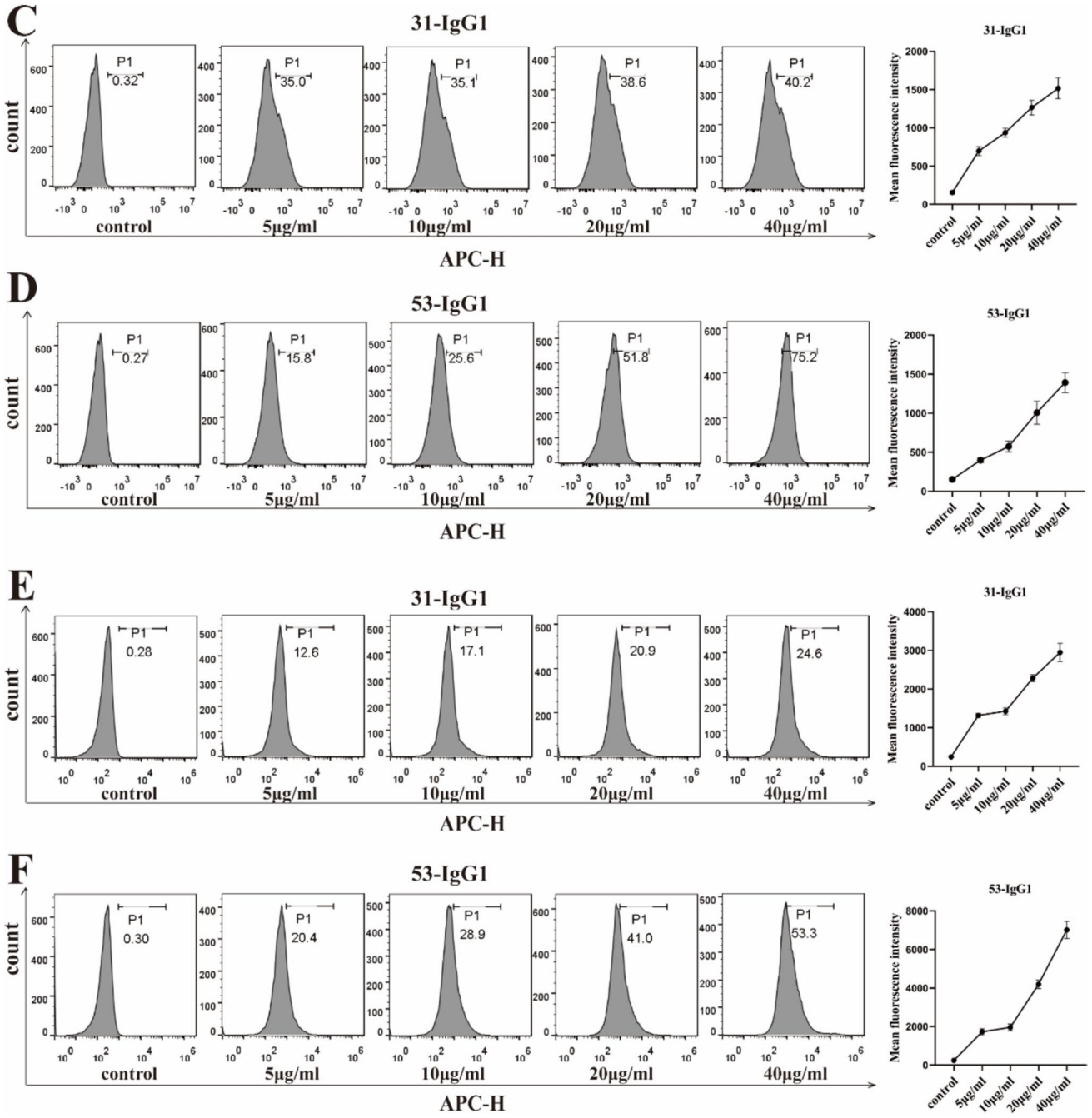

Fig. 5 (continued)

of 75.2%. Similarly, the binding results with A549 cells overexpressing Nrp-1 are depicted in Fig. 5e–f: 31-IgG1 displayed a maximum binding rate of 24.6% to A549 cells overexpressing Nrp-1, whereas 53-IgG1 achieved a maximum binding rate of 53.3% to A549 cells overexpressing Nrp-1. These findings demonstrate the effective binding of both anti-Nrp-1 antibodies to Nrp-1 on the cell surface, with the binding rate and average fluorescence intensity positively correlated with antibody concentration.

Effects of anti-Nrp-1 IgG1 on memory T cells and analysis of antitumor activity in vitro

To evaluate the effect of anti-Nrp-1 IgG1 antibody on $CD8^+$ memory T cells, we performed a cell memory assay using $CD8^+$ T cells from malignant pleural effusions of lung adenocarcinoma patients. The gating strategy of memory T cell subpopulations in $CD8^+$ T cells was determined by flow cytometry (Fig. 6a). The results showed that naïve T cells

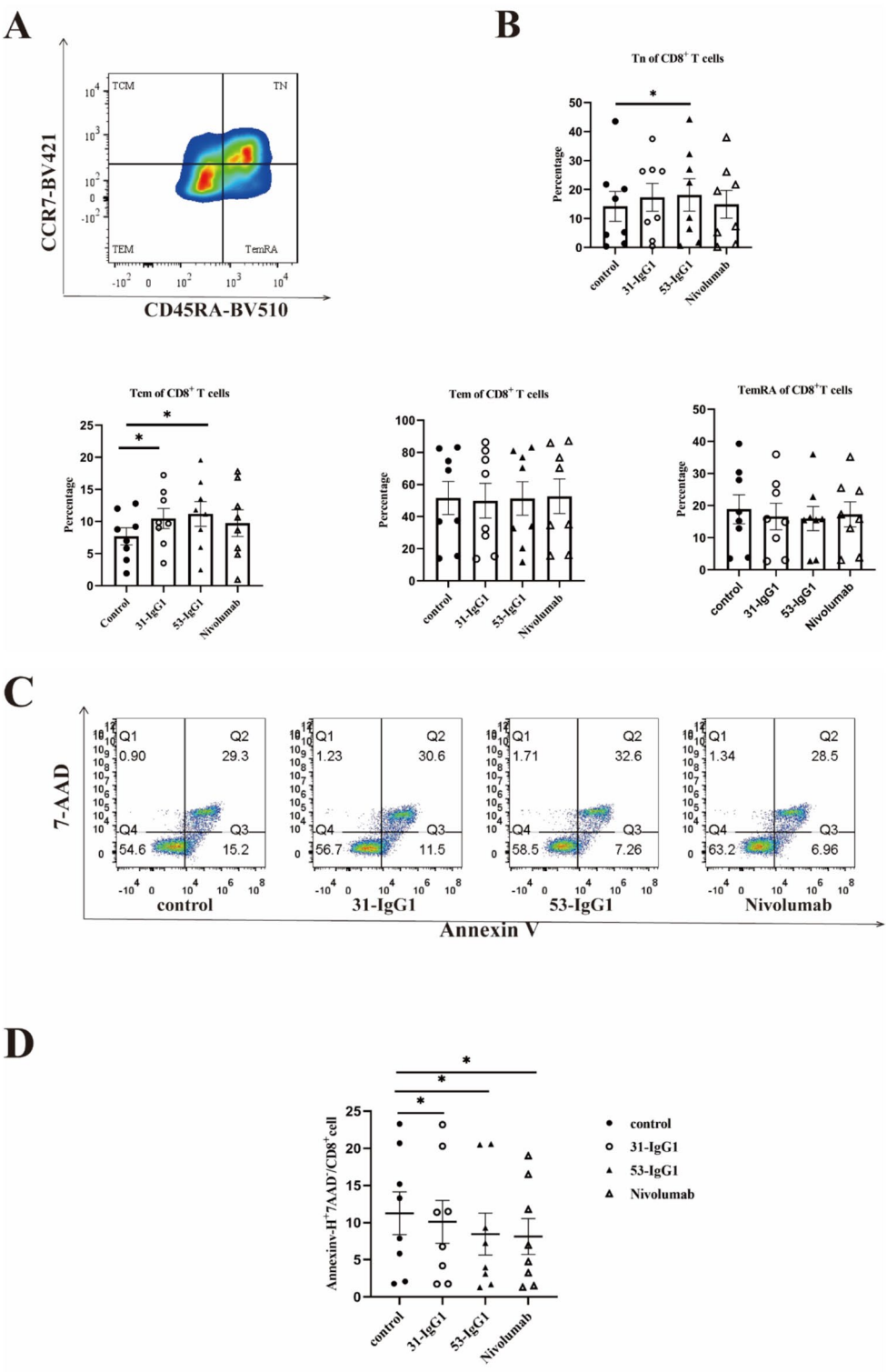

Fig. 6 Analysis of antitumor function and T cell memory of anti-Nrp-1 IgG1 antibody. **a** Gating strategy for memory T cell subsets in $CD8^+$ T cells in malignant pleural effusions from patients with lung adenocarcinoma. Memory T cells were defined as naïve T cells ($CD45RA^+$ $CCR7^+$), central memory T cells ($CD45RA^-$ $CCR7^+$), effector memory T cells ($CD45RA^-$ $CCR7^-$), and terminally differentiated effector memory T cells ($CD45RA^+$ $CCR7^-$). **b** Percentage of naïve T cells (TN), central memory (TCM), effector memory (TEM), and effector memory RA (TEMRA) T cells in pleural effusions of lung adenocarcinoma patients by anti-Nrp-1 IgG1 (40 μg/mL). **c** Effect of anti-Nrp-1 IgG1 (40 μg/mL) on apoptosis of $CD8^+$ T cells in pleural fluid from patients with lung adenocarcinoma, as analyzed by cell flow scatter plot. **d** Percentage of Annexin V^+ 7-AAD^- cells (early apoptosis) among $CD8^+$ T cells. Patients with lung adenocarcinoma $n=8$. **e** Effect of anti-Nrp-1 IgG1 (40 μg/mL) on apoptosis of A459 cells in the co-culture system, as analyzed by a flow scatter plot of apoptotic target cells. **f** Percentage of Annexin V^+ 7-AAD^+ cells (late apoptosis) among A549 cells. Healthy donors $n=6$. $^*P<0.05$, $^{**}P<0.01$, $^{***}P<0.001$

were higher in the CD8 subpopulation of the experimental group treated with 53 Nrp1-IgG1 than in the negative control group, and central memory T cells were higher in the CD8 subpopulation of 31 Nrp-IgG1 and 53 Nrp1-IgG1 than in the negative control group (Fig. 6b). Then, we conducted an apoptosis assay using $CD8^+$ T cells from malignant pleural fluid obtained from patients with lung adenocarcinoma. The experimental results, as shown in Fig. 6c–d, revealed that the Annexin V^+ 7-AAD^- cell frequencies for both 31 Nrp1-IgG1 and 53 Nrp1-IgG1 were significantly lower in

Fig. 6 (continued)

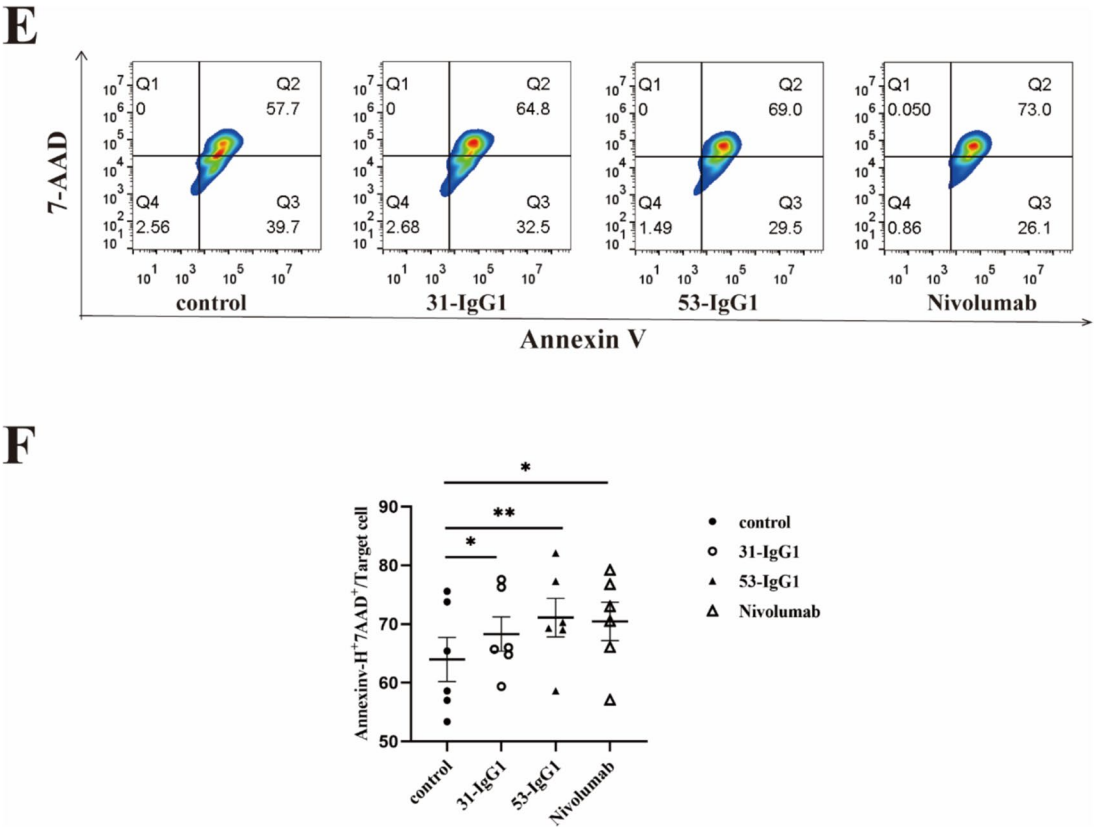

the experimental group compared with the Annexin V^+ 7-AAD^- cell frequencies in the negative control group. Notably, the experimental group exhibited similar frequencies to the positive control group treated with nivolumab Annexin V^+ 7-AAD^-. These results indicate that the anti-Nrp1-IgG1 antibody had a restorative effect on the early apoptosis of exhausted $CD8^+$ T cells, and 53 Nrp1-IgG1 was more effective than 31 Nrp1-IgG1.

The CCK8 method was used to detect the direct effect of the anti-Nrp1-IgG1 antibody on A549 cells, and it was found that the antibody could not directly inhibit the proliferation of tumor cells (Fig S4a-S4b), and there was no obvious trend of change in the survival rate of tumor cells with the increase in antibody concentration. Previously, we observed Nrp-1 expression on activated $CD8^+$ T cells. Therefore, we examined the apoptosis of A549 target cells after PBMCs from healthy donors were stimulated with anti-CD3/CD28 antibodies for 3 days. Stimulated PBMCs were subsequently co-cultured with A549 tumor cells in the presence or absence of anti-Nrp1-IgG1 antibody for 48 h. The results, as displayed in Fig. 6e–f, indicated an increased Annexin V^+ 7-AAD^+ cell frequency in the experimental groups treated with both 31 Nrp1-IgG1 and 53 Nrp1-IgG1 compared with the negative control group. These findings suggest that anti-Nrp1-IgG enhanced the killing effect of PBMCs on A549 target cells in the co-culture system, leading to increased late-stage apoptosis of target cells. Furthermore, 53 Nrp1-IgG1 demonstrated a stronger killing effect than 31 Nrp1-IgG1.

In vivo analysis of antitumor activity of anti-Nrp1-IgG1 antibody

In in vitro cell function assays, Jurkat T and A549 cells overexpressing Nrp-1 displayed superior binding activity with 53 IgG1 antibody and exhibited stronger antitumor activity. Therefore, we selected 53 IgG1 for in vivo antitumor activity analysis. Given that 53 IgG1 is a fully human antibody, its in vivo functionality was initially verified using an immune system-humanized lung cancer mouse model. This model involved subcutaneously injecting A549 cells, followed by the intravenous injection of human PBMCs when the tumor volume reached 80 mm^3. Antibody administration began the next day, with a total of five administrations. Blood samples obtained from mouse orbits were assessed for humanization of the mouse immune system. The results (Fig. 7a) indicated that the percentage of $hCD45^+$ cells in the peripheral blood of PBMC humanized tumor transplant mouse model ranged from 34.9% to 76.4% (Successful humanized immune system of mice is defined as 25% or more human $CD45^+$ cells in mouse peripheral blood mononuclear cells) (25) [26], confirming the successful construction of a mouse model with a humanized immune system.

Analyzing the changes in tumor weight and volume in mice, we observed a significant reduction in tumor volume and tumor weight in the 53-IgG1 experimental group (Fig. 7b–c). In addition, we observed a slight loss of body weight of mice, but there was no significant difference, and no significant adverse effects were observed. (Fig. 7d) This suggests that the 53-IgG1 antibody had a certain inhibitory effect on the growth of mouse lung cancer tumors. Subsequently, we analyzed TILs from tumor tissues in the mouse model with a humanized immune system. Flow cytometry results (Fig. 7e–f) revealed significantly higher counts of $CD8^+$ T cells and $CD3^+CD45^+$ cells in the tumor tissues of the 53-IgG1 experimental group compared to the human IgG1 control group.

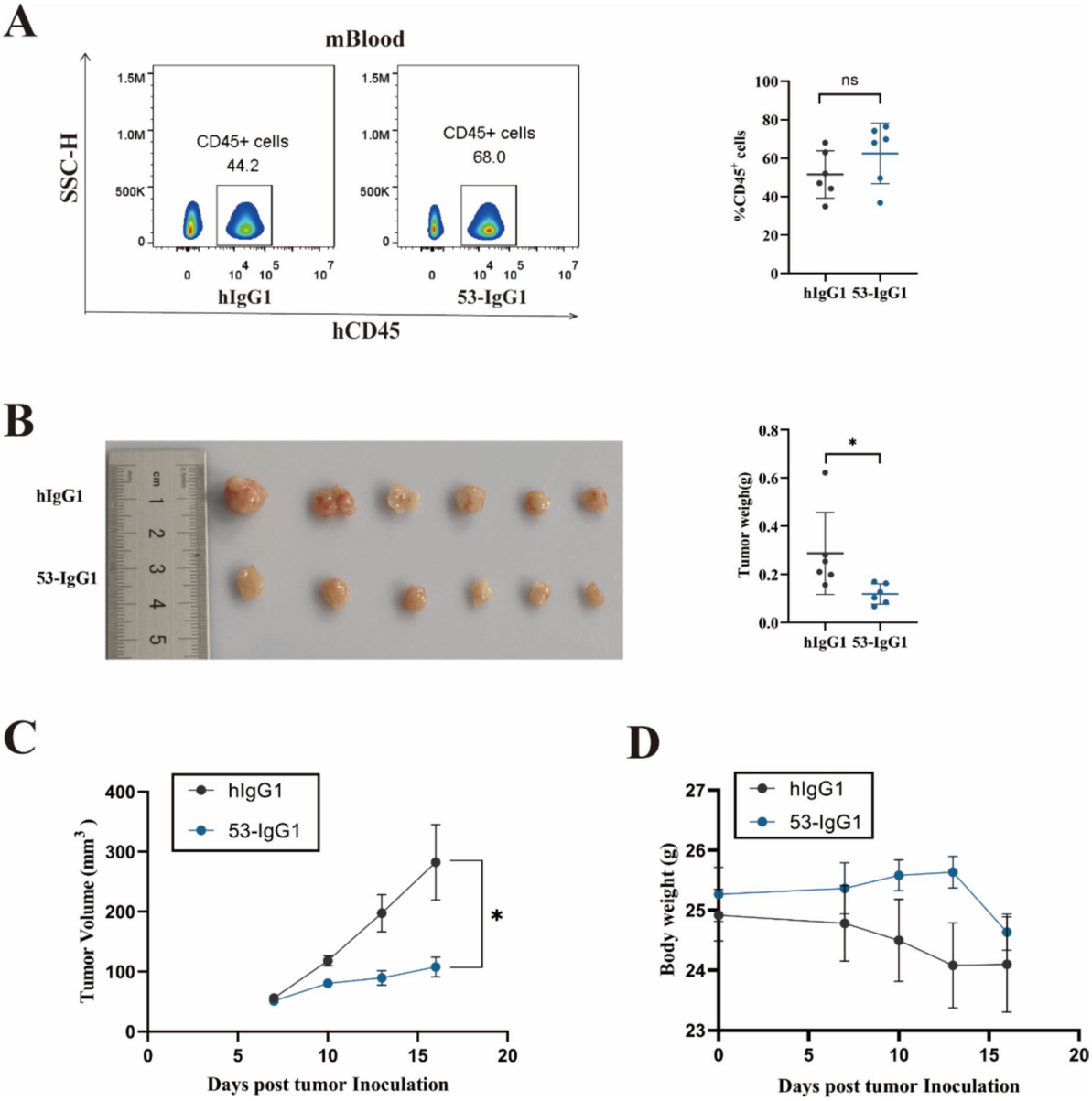

Fig. 7 Establishment of a humanized lung cancer model of the immune system and tumor inhibition by anti-Nrp-1 IgG1 antibody. **a** Left: Peripheral blood $hCD45^+$ flow scatter plot analysis in the mouse immune system-humanized lung cancer model; Right: Percentage of hCD45 in peripheral blood cells. **b** Left: Changes in mice tumor solid mass; Right: Analysis of mouse tumor weight. **c** Changes in tumor volume in mice inoculated with A549 tumor cells **d**. Changes in body weight of mice inoculated with A549 tumor cells **e** Left: Flow scatter plot analysis of $hCD8^+$ T cells in the TILs of tumor tissues from a mouse immune system-humanized lung cancer model; Right: Percentage of $CD8^+$ cells in the TILs. **f** Left: Flow scatter plot analysis of $hCD45^+$ T cells in the TILs of tumor tissues from a mouse immune system-humanized lung cancer model; Right: Percentage of $CD45^+$ cells in the TILs. The experimental and control mice were $n=6$, respectively. $^*P<0.05$, $^{**}P<0.01$, and $^{***}P<0.001$, $^{****}P<0.0001$

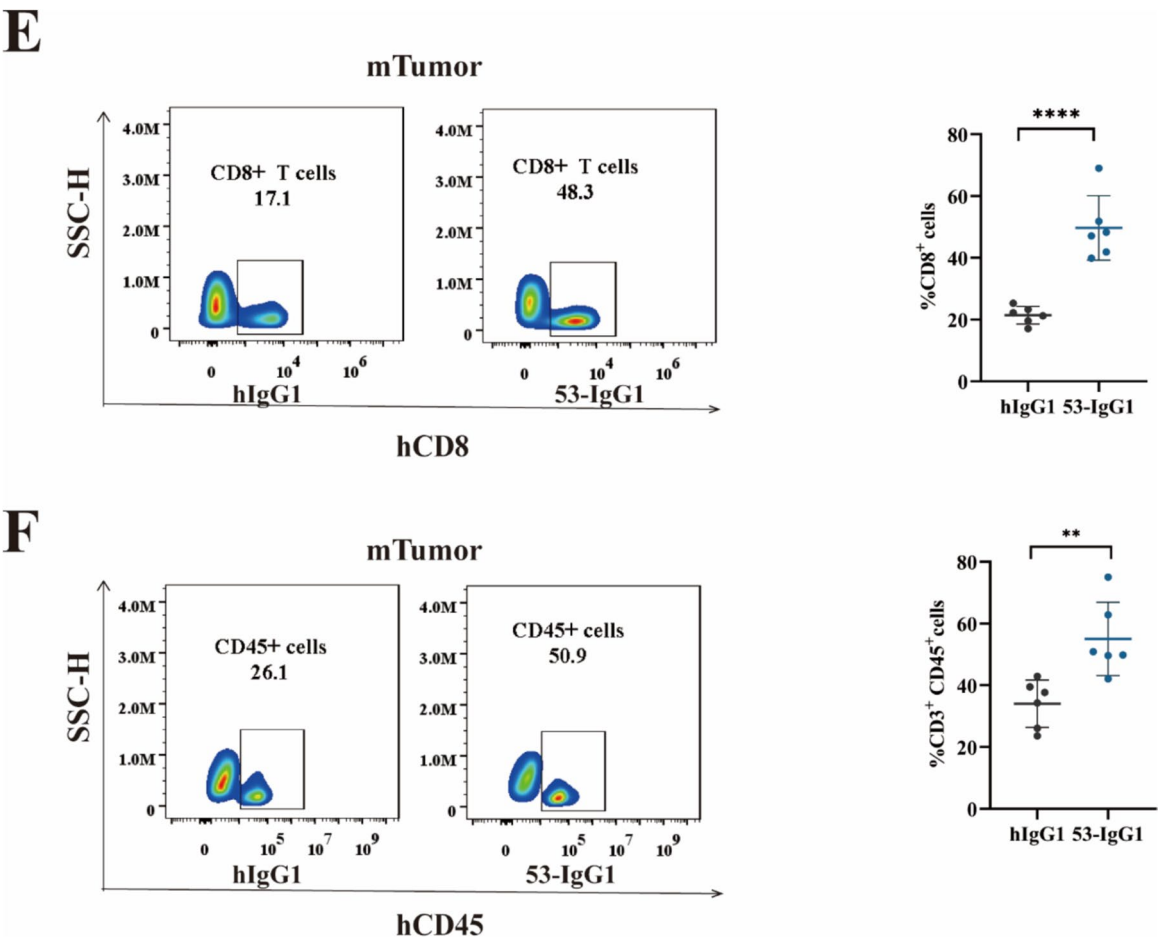

Fig. 7 (continued)

Discussion

In recent years, immune checkpoint blockade therapy has gained widespread usage in the clinical treatment of malignant tumors. Yet, the antitumor potential of Nrp-1, functioning as an immune checkpoint in conjunction with fully human IgG antibodies, remains a subject awaiting comprehensive exploration. In our current study, we initiated our investigation by establishing that the expression of the Nrp-1 gene exhibited significantly higher levels within TIL $CD8^+$ T cells derived from patients with lung adenocarcinoma compared with its prevalence in PBMCs. Simultaneously, we leveraged 20 lymphoid tissues from distinct patients with NSCLC as the foundational elements for constructing scFv libraries with ample capacity and substantial diversity. Subsequently, we meticulously screened the library to identify scFv molecules demonstrating high affinity for Nrp-1 as our target of interest, ultimately transforming them into full-length IgG1 antibodies. Through in vitro experimentation, we observed that the anti-Nrp-1 IgG1 antibody was effective in restoring the partial killing function of exhausted $CD8^+$ T cells isolated from the malignant pleural fluid of lung adenocarcinoma patients. Furthermore, in co-culture experiments, the same antibody remarkably enhanced the cytotoxicity of PBMCs against target cells. Finally, we established an immune system-humanized lung cancer mouse model, where 53-IgG1 demonstrated substantial tumor inhibition. Within the realm of cancer immunotherapy, 53-IgG1 is poised to become a promising agent for targeting Nrp-1.

Numerous studies have established a close correlation between elevated Nrp-1 expression and key aspects of tumorigenesis, including progression, invasion, metastasis, and prognosis [27–31]. Nrp-1 not only promotes tumor angiogenesis and progression [32], but it is also widely expressed in a variety of tumor cell types, including malignant melanoma, malignant glioma, lung cancer, and gastric cancer, and its expression is often associated with poor prognosis [27, 33–35]. Moreover, Nrp-1 was found to be more prevalent in TIL $CD8^+$ T cells derived from patients with lung adenocarcinoma compared with their PBMCs counterparts, potentially indicating a link between Nrp-1 and $CD8^+$ T cell exhaustion. Thus, in this study, we constructed a fully human

phage single-chain antibody library from lymphoid tissues originating from lung cancer. These antibodies underwent affinity maturation within patients, simplifying the screening process for high-affinity anti-Nrp-1 scFv within the library. The scFvs we screened are fully human antibodies, and therefore may be less immunogenic in vivo than the mouse or chimeric antibodies. Notably, while scFv possesses a short half-life and is susceptible to inactivation, full-length IgG boasts a molecular weight of approximately 150 kDa and enjoys a blood clearance half-life of 21 days in vivo [36, 37]. Most therapeutic antibody drugs available today have been developed based on an IgG framework, with the majority belonging to the IgG1 subtype [38, 39]**.** IgG1 isoforms account for 60% of serum distribution, binding to protein antigens with remarkable stability and minimal polymerization tendencies [40, 41]. Hence, the anti-Nrp-1 scFv was converted into a full-length IgG1 antibody for application in this study.

Studies had shown that anti-Nrp-1 immunotherapy was effective in preventing melanoma progression in C57BL/6 mice. Additionally, combining anti-Nrp-1 antibody with anti-PD-1 antibody demonstrated superior efficacy in inhibiting tumor growth, with no cumulative effect on T cell-mediated cytotoxicity in isolated cells. Inhibition of Nrp-1 may be a potential therapeutic strategy to improve anti-PD1 efficacy [42]. The antibodies developed in our study were fully humanized and their antitumor capabilities were assessed by constructing a mouse model of lung cancer with a humanized immune system to avoid potential immune rejection. The results showed that the reduction in tumor growth in vivo was associated with an increased in $CD8^+$ effector T cells infiltration into the tumor, which may be related to the ability of the anti-Nrp-1 antibody to promote T cell migration and recruitment in the tumor microenvironment. It has been suggested that Nrp-1 expression in CD8 T cells may affect the persistence of CD8 T cell-mediated tumor immunosurveillance, and Nrp-1 may impede the development of long-lasting tumor-specific T cells; thus, blocking Nrp-1, a unique "immune memory checkpoint," may promote the development of long-lasting tumor-specific memory T cells [13]. Furthermore, no significant weight loss or adverse effects were observed in mice following the administration of anti-Nrp-1 IgG1 antibody in the in vivo model. To mitigate potential antibody-dependent cell-mediated or complement-dependent cytotoxicity that may result from long-term dosing, follow-up work will involve the development of anti-Nrp-1 IgG4 antibodies and comparative studies of its antitumor function and side effects with the anti-Nrp-1 IgG1 antibody. Despite our antibodies were developed as mAbs, these antibodies could also be used as antibody platforms for generating bispecific antibody or combination therapies for the effective treatment of NSCLC patients. In conclusion, the 53-IgG antibody generated in our study holds promise as a monoclonal antibody for the treatment of lung cancer. However, we must also acknowledge the limitations of our study, as the molecular mechanisms underlying the antitumor activity of 53-IgG antibody remains unresolved and needs to be further explored in future studies.

Conclusion

Collectively, this study has identified novel anti–Nrp-1 antibody candidate molecule 53-IgG1, which has been tested and shown to have excellent in vitro biologic activity. At the same time, therapy offers a certain level of in vivo antitumor activity. 53-IgG1 is expected to be the most promising potential candidate for targeting Nrp-1 for NSCLC treatment.

Supplementary Information The online version contains supplementary material available at https://doi.org/10.1007/s00262-024-03893-1.

Acknowledgements This work was supported by the project of Science and Technology Department of Sichuan Province (2023NSFSC0727, 2025NSFSC0898); the Sichuan Science and Technology program (2022YFS0630-B3); the project Luzhou Science and Technology Bureau (2023LZXNYDJ020, 2023SYF100, 2024SYF128).

Author contributions BZ and QL designed the study. BZ completed the cell experiments and wrote the article. QL completed the data analysis, and processed the images. LL,YY, XG and LC were involved in study implementation, acquisition and analysis. WX and XM jointly analyzed the animal models. SN and QY supervised the study. All authors contributed to drafting of the manuscript and approved the final version.

Data availability No datasets were generated or analyzed during the current study.

Declarations

Conflict of interest The authors declare no competing interests.

Ethical approval All in vivo animal experiments were approved by the Committee on the Ethics of Animal Experiments of Southwest Medical University (20220812–030). The clinical experiment was approved by the Experimental Ethics Committee of the Affiliated Hospital of Southwest Medical University (KY2023277).

References

1. Miller M, Hanna N (2021) Advances in systemic therapy for non-small cell lung cancer. BMJ 375:n2363. https://doi.org/10.1136/bmj.n2363
2. Xia L, Liu Y, Wang Y (2019) PD-1/PD-L1 blockade therapy in advanced non-small-cell lung cancer: current status and future directions. Oncologist 24:S31-s41. https://doi.org/10.1634/theoncologist.2019-IO-S1-s05
3. Pardoll DM (2012) The blockade of immune checkpoints in cancer immunotherapy. Nat Rev Cancer 12:252–264. https://doi.org/10.1038/nrc3239
4. Passaro A, Brahmer J, Antonia S, Mok T, Peters S (2022) Managing resistance to immune checkpoint inhibitors in lung cancer: treatment and novel strategies. J Clin Oncol Off J Am Soc Clin Oncol 40:598–610. https://doi.org/10.1200/jco.21.01845
5. Lee WS, Yang H, Chon HJ, Kim C (2020) Combination of anti-angiogenic therapy and immune checkpoint blockade normalizes vascular-immune crosstalk to potentiate cancer immunity. Exp Mol Med 52:1475–1485. https://doi.org/10.1038/s12276-020-00500-y
6. Cimato T, Beers J, Ding S, Ma M, McCoy JP, Boehm M, Nabel EG (2009) Neuropilin-1 identifies endothelial precursors in human and murine embryonic stem cells before CD34 expression. Circulation 119:2170–2178. https://doi.org/10.1161/circulationaha.109.849596
7. Kawasaki T, Kitsukawa T, Bekku Y, Matsuda Y, Sanbo M, Yagi T, Fujisawa H (1999) A requirement for neuropilin-1 in embryonic vessel formation. Develop (Cambridge, England) 126:4895–4902. https://doi.org/10.1242/dev.126.21.4895
8. Kitsukawa T, Shimizu M, Sanbo M, Hirata T, Taniguchi M, Bekku Y, Yagi T, Fujisawa H (1997) Neuropilin-semaphorin III/D-mediated chemorepulsive signals play a crucial role in peripheral nerve projection in mice. Neuron 19:995–1005. https://doi.org/10.1016/s0896-6273(00)80392-x
9. Gu C, Rodriguez ER, Reimert DV, Shu T, Fritzsch B, Richards LJ, Kolodkin AL, Ginty DD (2003) Neuropilin-1 conveys semaphorin and VEGF signaling during neural and cardiovascular development. Dev Cell 5:45–57. https://doi.org/10.1016/s1534-5807(03)00169-2
10. Roy S, Bag AK, Singh RK, Talmadge JE, Batra SK, Datta K (2017) Multifaceted role of neuropilins in the immune system: potential targets for immunotherapy. Front Immunol 8:1228. https://doi.org/10.3389/fimmu.2017.01228
11. Jung K, Kim JA, Kim YJ, Lee HW, Kim CH, Haam S, Kim YS (2020) A neuropilin-1 antagonist exerts antitumor immunity by inhibiting the suppressive function of intratumoral regulatory T cells. Cancer Immunol Res 8:46–56. https://doi.org/10.1158/2326-6066.Cir-19-0143
12. Battaglia A, Buzzonetti A, Monego G, Peri L, Ferrandina G, Fanfani F, Scambia G, Fattorossi A (2008) Neuropilin-1 expression identifies a subset of regulatory T cells in human lymph nodes that is modulated by preoperative chemoradiation therapy in cervical cancer. Immunol 123:129–138. https://doi.org/10.1111/j.1365-2567.2007.02737.x
13. Liu C, Somasundaram A, Manne S et al (2020) Neuropilin-1 is a T cell memory checkpoint limiting long-term antitumor immunity. Nat Immunol 21:1010–1021. https://doi.org/10.1038/s41590-020-0733-2
14. Weekes CD, Beeram M, Tolcher AW et al (2014) A phase I study of the human monoclonal anti-NRP1 antibody MNRP1685A in patients with advanced solid Tumors. Invest New Drugs 32:653–660. https://doi.org/10.1007/s10637-014-0071-z
15. Yuan Q, Huang L, Wang X, Wu Y, Gao Y, Li C, Nian S (2012) Construction of human nonimmune library and selection of scFvs against IL-33. Appl Biochem Biotechnol 167:498–509. https://doi.org/10.1007/s12010-012-9676-x
16. Suarez GV, Melucci Ganzarain CDC, Vecchione MB, Trifone CA, Marín Franco JL, Genoula M, Moraña EJ, Balboa L, Quiroga MF (2019) PD-1/PD-L1 pathway modulates macrophage susceptibility to mycobacterium tuberculosis specific CD8(+) T cell induced death. Sci Rep 9:187. https://doi.org/10.1038/s41598-018-36403-2
17. Judge SJ, Darrow MA, Thorpe SW et al (2020) Analysis of tumor-infiltrating NK and T cells highlights IL-15 stimulation and TIGIT blockade as a combination immunotherapy strategy for soft tissue sarcomas. J Immun Cancer 8:1355. https://doi.org/10.1136/jitc-2020-001355
18. Daftarian PM, King J, Goverse G, Kleiman E (2023) An in vitrot cell dysfunction/exhaustion assay system that is partially reversible by pembrolizumab. J Immunol 210:245. https://doi.org/10.4049/jimmunol.210.Supp.245.23
19. Ye G, Sun X, Li J, Mai Y, Gao R, Zhang J (2023) Secondary metabolites of mulberry leaves exert anti-lung cancer activity through regulating the PD-L1/PD-1 signaling pathway. J Pharm Anal 16:100926. https://doi.org/10.1016/j.jpha.2023.12.016
20. Wang CI, Chang YF, Sie ZL, Ho AS, Chang JS, Peng CL, Cheng CC (2021) Irradiation suppresses IFNγ-mediated PD-L1 and MCL1 expression in EGFR-positive lung cancer to augment CD8(+) T cells cytotoxicity. Cells 10:515. https://doi.org/10.3390/cells10102515
21. Davern M, Donlon NE, O'Connell F et al (2023) Nutrient deprivation and hypoxia alter T cell immune checkpoint expression: potential impact for immunotherapy. J Cancer Res Clin Oncol 149:5377–5395. https://doi.org/10.1007/s00432-022-04440-0
22. Sung E, Ko M, Won JY et al (2022) LAG-3xPD-L1 bispecific antibody potentiates antitumor responses of T cells through dendritic cell activation. Mol Ther J Am Soc Gene Therapy 30:2800–2816. https://doi.org/10.1016/j.ymthe.2022.05.003
23. Lin S, Huang G, Cheng L et al (2018) Establishment of peripheral blood mononuclear cell-derived humanized lung cancer mouse models for studying efficacy of PD-L1/PD-1 targeted immunotherapy. mAbs 10:1301–11. https://doi.org/10.1080/19420862.2018.1518948
24. Pyo KH, Kim JH, Lee JM, Kim SE, Cho JS, Lim SM, Cho BC (2019) Promising preclinical platform for evaluation of immuno-oncology drugs using Hu-PBL-NSG lung cancer models. Lung Cancer 127:112–121. https://doi.org/10.1016/j.lungcan.2018.11.035
25. Park N, Pandey K, Chang SK et al (2020) Preclinical platform for long-term evaluation of immuno-oncology drugs using hCD34+ humanized mouse model. J Immun Cancer 8:1513. https://doi.org/10.1136/jitc-2020-001513
26. Xu X, Gu H, Li H et al (2022) Large-cohort humanized NPI mice reconstituted with CD34(+) hematopoietic stem cells are feasible for evaluating preclinical cancer immunotherapy. FASEB J Off Publ Feder Am Soc Experim Biol 36:e22244. https://doi.org/10.1096/fj.202101548RR
27. Hang C, Yan HS, Gong C, Gao H, Mao QH, Zhu JX (2019) MicroRNA-9 inhibits gastric cancer cell proliferation and migration by targeting neuropilin-1. Exp Ther Med 18:2524–2530. https://doi.org/10.3892/etm.2019.7841
28. Zhou R, Curry JM, Roy LD et al (2016) A novel association of neuropilin-1 and MUC1 in pancreatic ductal adenocarcinoma: role in induction of VEGF signaling and angiogenesis. Oncogene 35:5608–5618. https://doi.org/10.1038/onc.2015.516

29. Hendricks C, Dubail J, Brohée L, Delforge Y, Colige A, Deroanne C (2016) A novel physiological glycosaminoglycan-deficient splice variant of neuropilin-1 Is anti-tumorigenic in vitro and in vivo. PLoS ONE 11:e0165153. https://doi.org/10.1371/journal.pone.0165153
30. Al-Shareef H, Hiraoka SI, Tanaka N, Shogen Y, Lee AD, Bakhshishayan S, Kogo M (2016) Use of NRP1, a novel biomarker, along with VEGF-C, VEGFR-3, CCR7 and SEMA3E, to predict lymph node metastasis in squamous cell carcinoma of the tongue. Oncol Rep 36:2444–2454. https://doi.org/10.3892/or.2016.5116
31. Jimenez-Hernandez LE, Vazquez-Santillan K, Castro-Oropeza R et al (2018) NRP1-positive lung cancer cells possess tumor-initiating properties. Oncol Rep 39:349–357. https://doi.org/10.3892/or.2017.6089
32. Sarabipour S, Mac Gabhann F (2018) VEGF-A121a binding to neuropilins - a concept revisited. Cell Adh Migr 12:204–214. https://doi.org/10.1080/19336918.2017.1372878
33. Soker S, Takashima S, Miao HQ, Neufeld G, Klagsbrun M (1998) Neuropilin-1 is expressed by endothelial and tumor cells as an isoform-specific receptor for vascular endothelial growth factor. Cell 92:735–745. https://doi.org/10.1016/s0092-8674(00)81402-6
34. Hu B, Guo P, Bar-Joseph I et al (2007) Neuropilin-1 promotes human glioma progression through potentiating the activity of the HGF/SF autocrine pathway. Oncogene 26:5577–5586. https://doi.org/10.1038/sj.onc.1210348
35. Wang L, Sun M, Lin X, Lei Y, Yin Z, Zhou W (2021) Down-regulation of HBXIP inhibits non-small cell lung cancer growth and enhances the anti-tumor immunity of mice by reducing NRP-1. Ann Clin Lab Sci 51:487–493
36. Duan Y, Chen R, Huang Y et al (2021) Tuning the ignition of CAR: optimizing the affinity of scFv to improve CAR-T therapy. Cellu Mol Life Sci CMLS 79:14. https://doi.org/10.1007/s00018-021-04089-x
37. Ferl GZ, Kenanova V, Wu AM, DiStefano JJ 3rd (2006) A two-tiered physiologically based model for dually labeled single-chain Fv-Fc antibody fragments. Mol Cancer Ther 5:1550–1558. https://doi.org/10.1158/1535-7163.Mct-06-0072
38. Yu J, Song Y, Tian W (2020) How to select IgG subclasses in developing anti-tumor therapeutic antibodies. J Hematol Oncol 13:45. https://doi.org/10.1186/s13045-020-00876-4
39. Vukovic N, van Elsas A, Verbeek JS, Zaiss DMW (2021) Isotype selection for antibody-based cancer therapy. Clin Exp Immunol 203:351–365. https://doi.org/10.1111/cei.13545
40. Maia J, Otake AH, Poças J, Carvalho AS, Beck HC, Magalhães A, Matthiesen R, Strano Moraes MC, Costa-Silva B (2020) Transcriptome reprogramming of CD11b(+) bone marrow cells by pancreatic cancer extracellular vesicles. Front Cell Develop Biol 8:592518. https://doi.org/10.3389/fcell.2020.592518
41. Yang B, Zhang Z, Chen X et al (2022) An Asia-specific variant of human IgG1 represses colorectal tumorigenesis by shaping the tumor microenvironment. J Clin Invest 132:153454. https://doi.org/10.1172/jci153454
42. Rossignol J, Belaid Z, Fouquet G et al (2022) Neuropilin-1 cooperates with PD-1 in CD8(+) T cells predicting outcomes in melanoma patients treated with anti-PD1. iScience 25:104353. https://doi.org/10.1016/j.isci.2022.104353